

Search for $K^+ \rightarrow \pi^+ \nu \bar{\nu}$ at NA62

Matthew Moulson* for the NA62 Collaboration[†]

INFN Laboratori Nazionali di Frascati, Italy

E-mail: moulson@lnf.infn.it

The decay $K^+ \rightarrow \pi^+ \nu \bar{\nu}$ is highly suppressed in the Standard Model (SM), while its rate can be predicted with minimal theoretical uncertainty. The branching ratio (BR) for this decay is thus a sensitive probe of the flavor sector of the SM; its measurement, however, is a significant experimental challenge. The primary goal of the NA62 experiment is to measure $\text{BR}(K^+ \rightarrow \pi^+ \nu \bar{\nu})$ with 10% precision. NA62 took data in pilot runs in 2014 and 2015, reaching the design beam intensity. The status of the experiment and the prospects for the measurement of $\text{BR}(K^+ \rightarrow \pi^+ \nu \bar{\nu})$ are presented.

38th International Conference on High Energy Physics

3-10 August 2016

Chicago, USA

*Speaker.

[†]G. Aglieri Rinella, R. Aliberti, F. Ambrosino, R. Ammendola, B. Angelucci, A. Antonelli, G. Anzivino, R. Arcidiacono, I. Azhinenko, S. Balev, M. Barbanera, J. Bendotti, A. Biagioni, L. Bician, C. Biino, A. Bizzeti, T. Blazek, A. Blik, B. Bloch-Devaux, V. Bolotov, V. Bonaiuto, M. Boretto, M. Bragadireanu, D. Britton, G. Britvich, M.B. Brunetti, D. Bryman, F. Bucci, F. Butin, J. Calvo, E. Capitolo, C. Capocchia, T. Capussela, A. Cassese, A. Catinaccio, A. Cecchetti, A. Ceccucci, P. Cenci, V. Cerny, C. Cerri, B. Checcucci, O. Chikilev, S. Chiozzi, R. Ciaranfi, G. Collazuol, A. Conovaloff, P. Cooke, P. Cooper, G. Corradi, E. Cortina Gil, F. Costantini, F. Cotorobai, A. Cotta Ramusino, D. Coward, G. D'Agostini, J. Dainton, P. Dalpiaz, H. Danielsson, J. Degrange, N. De Simone, D. Di Filippo, L. Di Lella, S. Di Lorenzo, N. Dixon, N. Doble, B. Dobrich, V. Duk, V. Elsha, J. Engelfried, T. Enik, N. Estrada, V. Falaleev, R. Fantechi, V. Fascianelli, L. Federici, S. Fedotov, M. Fiorini, J. Fry, J. Fu, A. Fucci, L. Fulton, S. Gallorini, S. Galeotti, E. Gamberini, L. Gatignon, G. Georgiev, A. Gianoli, M. Giorgi, S. Giudici, L. Glonti, A. Goncalves Martins, F. Gonnella, E. Goudzovski, R. Guida, E. Gushchin, F. Hahn, B. Hallgren, H. Heath, F. Herman, T. Husek, O. Hutanu, D. Hutchcroft, L. Iacobuzio, E. Iacopini, E. Imbergamo, O. Jamet, P. Jarron, E. Jones, T. Jones K. Kampf, J. Kaplon, V. Kekelidze, S. Kholodenko, G. Khorauli, A. Khotyantsev, A. Khudyakov, Yu. Kiryushin, A. Kleimenova, K. Kleinknecht, A. Kluge, M. Koval, V. Kozhuharov, M. Krivda, Z. Kucerova, Yu. Kudenko, J. Kunze, G. Lamanna, G. Latino, C. Lazzeroni, G. Lehmann-Miotto, R. Lenci, M. Lenti, E. Leonardi, P. Lichard, R. Lietava, V. Likhacheva, L. Litov, R. Lollini, D. Lomidze, A. Lonardo, M. Lupi, N. Lurkin, K. McCormick, D. Madigozhin, G. Maire, C. Mandeiro, I. Mannelli, G. Mannoichi, A. Mapelli, F. Marchetto, R. Marchevski, S. Martellotti, P. Massarotti, K. Massri, P. Matak, E. Maurice, M. Medvedeva, A. Mefodev, E. Menichetti, E. Minucci, M. Mirra, M. Misheva, N. Molokanova, J. Morant, M. Morel, M. Moulson, S. Movchan, D. Munday, M. Napolitano, I. Neri, F. Newson, A. Norton, M. Noy, G. Nuessle, T. Numao, V. Obraztsov, A. Ostankov, S. Padolski, R. Page, V. Palladino, G. Paoluzzi, C. Parkinson, E. Pedreschi, M. Pepe, F. Perez Gomez, M. Perrin-Terrin, L. Peruzzo, P. Petrov, F. Petrucci, R. Piandani, M. Piccini, D. Pietreanu, J. Pinzino, I. Polenkevich, L. Pontisso, Yu. Potrebenikov, D. Protopopescu, F. Raffaelli, M. Raggi, P. Riedler, A. Romano, P. Rubin, G. Ruggiero, V. Russo, V. Ryjov, A. Salamon, G. Salina, V. Samsonov, C. Santoni, G. Saracino, F. Sargeni, V. Semenov, A. Sergi, M. Serra, A. Shaikhiev, S. Shkarovskiy, I. Skillicorn, D. Soldi, A. Sotnikov, V. Sugonyaev, M. Sozzi, T. Spadaro, F. Spinella, R. Staley, A. Sturgess, P. Sutcliffe, N. Szilasi, D. Tagnani, S. Trilov, M. Valdata-Nappi, P. Valente, M. Vasile, T. Vassilieva, B. Velghe, M. Veltri, S. Venditti, P. Vicini, R. Volpe, M. Vormstein, H. Wahl, R. Wanke, P. Wertelaers, A. Winhart, R. Winston, B. Wrona, O. Yushchenko, M. Zamkovsky, A. Zinchenko.

1. Introduction

The $K \rightarrow \pi \nu \bar{\nu}$ decays are flavor-changing neutral current (FCNC) processes that probe the $s \rightarrow d \nu \bar{\nu}$ transition via the Z-penguin and box diagrams shown in Figure 1. They are highly GIM suppressed and their Standard Model (SM) rates are very small. For several reasons, the SM

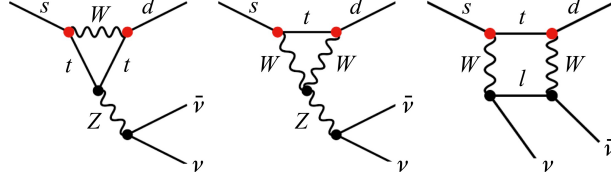


Figure 1: Diagrams contributing to the process $K \rightarrow \pi \nu \bar{\nu}$.

calculation for their branching ratios (BRs) is particularly clean: the loop amplitudes are dominated by the top-quark contributions, the hadronic matrix element for these decays can be obtained from the precise experimental measurement of the K_{e3} rate, and there are no long-distance contributions from processes with intermediate photons (see [1] for a review). In the SM, $\text{BR}(K^+ \rightarrow \pi^+ \nu \bar{\nu}) = (8.4 \pm 1.0) \times 10^{-11}$ and $\text{BR}(K_L \rightarrow \pi^0 \nu \bar{\nu}) = (3.4 \pm 0.6) \times 10^{-11}$ [2]. The uncertainties are entirely dominated by the CKM inputs, which in this case are from tree-level observables. Without these parametric errors, the uncertainties would be just 0.30×10^{-11} (3.5%) and 0.05×10^{-11} (1.5%), respectively. Because of corrections to the amplitudes from loops with the lighter quarks, the intrinsic uncertainty is slightly larger for the charged channel.

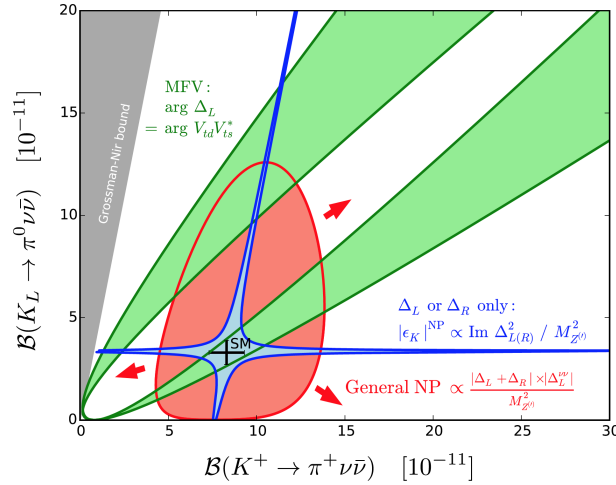


Figure 2: Schematic illustration of correlations between BRs for $K^+ \rightarrow \pi^+ \nu \bar{\nu}$ and $K_L \rightarrow \pi^0 \nu \bar{\nu}$ expected in different new-physics scenarios, from [3].

Because the SM rates are small and predicted very precisely, the BRs for these decays are sensitive probes for new physics. In general, $\text{BR}(K_L \rightarrow \pi^0 \nu \bar{\nu})$ and $\text{BR}(K^+ \rightarrow \pi^+ \nu \bar{\nu})$ are differently sensitive to modifications from a given new-physics scenario. If one or both BRs is found to differ from its SM value, it may be possible to characterize the physical mechanism responsible, as schematized in Figure 2, from [3]. For example, if the pattern of flavor-symmetry breaking from new physics were the same as in the SM (minimal flavor violation), the K_L and K^+ BRs would

lie along the band of correlation shown in green. If the new interaction were to couple to only left-handed or only right-handed quark currents, as expected for example in models with modified Z couplings or littlest Higgs models with T parity, the BRs would lie along one of the branches shown in blue. New physics without these constraints, as expected for example in models with large extra dimensions, could modify the K^+ and K_L BRs in an arbitrary way, as illustrated in red.

The decay $\text{BR}(K_L \rightarrow \pi^0 \nu \bar{\nu})$ has never been measured; the KOTO experiment at J-PARC [4] has a good chance of observing it. $\text{BR}(K^+ \rightarrow \pi^+ \nu \bar{\nu})$ has been measured by Brookhaven experiment E787 and its successor, E949. The combined result from the two generations of the experiment, obtained with seven candidate events, is $\text{BR}(K^+ \rightarrow \pi^+ \nu \bar{\nu}) = 1.73_{-1.05}^{+1.15} \times 10^{-10}$ [5]. The purpose of the NA62 experiment at the CERN SPS is to measure $\text{BR}(K^+ \rightarrow \pi^+ \nu \bar{\nu})$ with a precision of about 10%. After cuts, the signal detection efficiency for such decays is on the order of 10%, so observation of ~ 100 signal events will require a sample of 10^{13} K^+ decays within the geometrical acceptance of the experiment. For a measurement with 10% precision, the background level must be kept down to no more than about 20% of signal. This implies an overall background rejection factor of 10^{12} .

2. The NA62 experiment

The experimental signature for $K^+ \rightarrow \pi^+ \nu \bar{\nu}$ is a K^+ decaying to a π^+ , with no other particles present. The first line of defense against abundant decays such as $K^+ \rightarrow \mu^+ \nu$ and $K^+ \rightarrow \pi^+ \pi^0$ (together representing about 84% of the total K^+ width) is to precisely reconstruct the missing mass of the primary and secondary tracks and reject events with $m_{\text{miss}}^2 \approx 0$ or $m_{\text{miss}}^2 \approx m_{\pi^0}^2$, assuming the secondary is a μ^+ or a π^+ , respectively. However, the rejection power from kinematics alone is not sufficient (in NA62, it is at best 10^4), and in any case, about 8% of K^+ decays (e.g., K_{e3} , $K_{\mu 3}$) do not have closed kinematics. The remainder of the experiment's rejection power must come from redundant particle identification systems and hermetic, highly-efficient photon veto detectors. The NA62 apparatus [6], schematically illustrated in Figure 3, was designed around these principles, which we now consider in turn.

Beamline and decay volume The experiment makes use of a 400-GeV primary proton beam from the SPS with 3×10^{12} protons per pulse and a duty factor of about 0.3. The beam is collided on a beryllium target at zero angle to produce the 75-GeV $\pm 1\%$ unseparated positive secondary beam used by the experiment. At production, this beam consists of about 70% π^+ , 23% p , and 7% K^+ , with a total rate of 750 MHz. The beamline opens into the vacuum tank about 105 m downstream of the target. The vacuum tank is about 115 m long and fully encloses the four tracking stations of the magnetic spectrometer; the pressure inside is kept at a level of 10^{-6} mbar. The fiducial volume occupies the first 60 m of the vacuum tank, upstream of the spectrometer. About 10% of the K^+ 's entering the experiment decay in the fiducial volume, corresponding to 4.5 MHz of K^+ decays.

High-rate, precision tracking In order to obtain the full kinematic rejection factor of 10^4 for two-body decays, both the beam particle and the decay secondary must be accurately tracked. The beam spectrometer, referred to as the Gigatracker because it tracks individual particles in the 750-MHz secondary beam, consists of three hybrid silicon-pixel detectors installed in an achromat in the beamline [7]. The magnetic spectrometer for secondary particles consists of four straw chambers

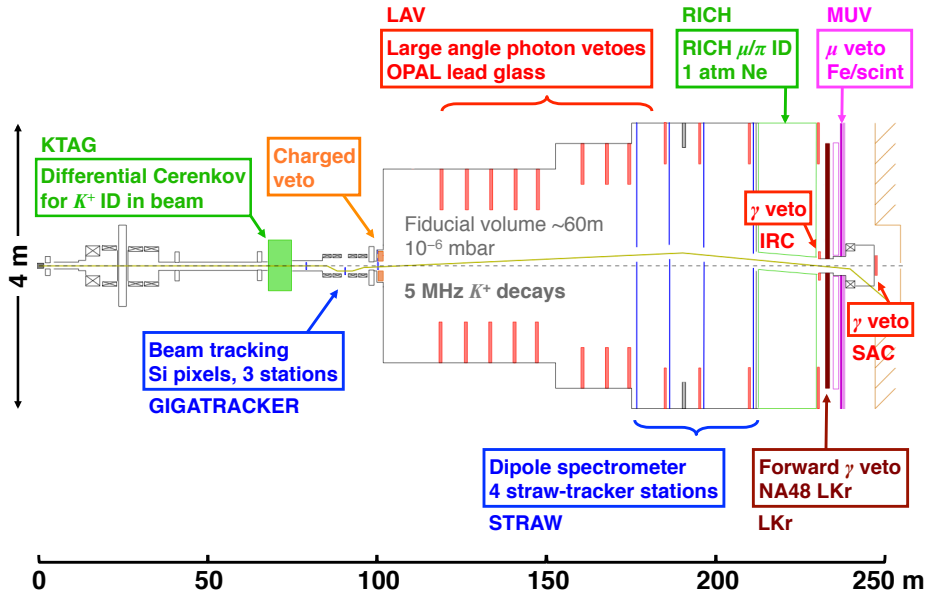


Figure 3: Schematic diagram of the NA62 experiment.

operated inside the vacuum tank [8]. Each chamber has 16 layers of straw tubes arranged in 4 views. A scintillator hodoscope downstream of the spectrometer allows fast ($\sigma_t \sim 200$ ps) low-level triggering on charged particles.

Redundant particle identification The principal PID challenge for single tracks is to reject $K^+ \rightarrow \mu^+ \nu$ decays with an inefficiency of less than 10^{-7} after the application of kinematic cuts. The bulk of NA62's π/μ separation capability is provided by the downstream muon vetoes (MUV). There are three MUV detectors. MUVs 1 and 2 are iron/scintillator hadron calorimeters. These are used mainly for offline π/μ separation and provide a muon rejection factor of 10^5 . MUV 3 is highly segmented and provides fast μ identification for triggering. An additional two orders of magnitude of π/μ separation are provided by a large (~ 4 -m-diameter by 17.5-m-long) ring-imaging Cerenkov counter (RICH) [9] filled with neon gas at 1 atm.

Beam timing and PID Considering that the rates of primary and secondary tracks in the experiment are respectively about 750 MHz and 10 MHz, accurately matching the correct secondary track to the correct primary is not a trivial task. Precise timing of the secondary can be obtained from the RICH ($\sigma_t \sim 100$ ps), while for the primary, the Gigatracker provides $\sigma_t \sim 150$ ps. The KTAG, a differential Cerenkov counter based on a CERN CEDAR-W detector that has been refurbished and outfitted with a new, high-segmentation readout [10], is used to identify kaons in the beam. This both provides a precise ($\sigma_t \sim 100$ ps), redundant measurement of the beam particle's timing and reduces the effective beam rate from 750 MHz to 45 MHz, hence reducing the mismatch probability.

Hermetic photon vetoes Rejection of photons from π^0 's is important for the elimination of many background channels, $K^+ \rightarrow \pi^+ \pi^0$ decays in particular. For these decays, requiring the π^+ to have $p < 35$ GeV guarantees that the two photons from the π^0 have a total energy of 40 GeV.

If the missing-mass cuts provide a rejection power of 10^4 , the probability for the photon vetoes to miss both photons must be less than 10^{-8} . The photon veto system consists of four separate subdetector systems. The ring-shaped large-angle photon vetoes (LAVs) are placed at 12 locations along the vacuum volume and provide coverage for decay photons emitted at angles to the beam line (θ) between 8.5 and 50 mrad. The LAV detectors consist of rings of lead-glass blocks salvaged from the OPAL electromagnetic calorimeter barrel [11]. The NA48 liquid-krypton calorimeter (LKr), a quasi-homogeneous ionization calorimeter of depth $27X_0$ and transverse segmentation of $2 \times 2 \text{ cm}^2$ [12], vetoes forward ($1 \text{ mrad} < \theta < 8.5 \text{ mrad}$), high-energy photons. A ring-shaped shashlyk calorimeter (IRC) about the beamline provides coverage for photons with $\theta < 1 \text{ mrad}$, while further downstream, a small-angle shashlyk calorimeter (SAC) around which the beam is deflected completes the coverage for very-small-angle photons that would otherwise escape via the beam pipe.

Expected performance Simulations indicate that the acceptance for signal decays within the fiducial volume is around 10%, corresponding to about 45 signal events accepted per year of data taking. The $\pi^+\pi^0$ background is estimated to be about 10% of signal counts, while the $\mu^+\nu$ background is around 3%. Including backgrounds from all other channels, the total background is under 20%.

3. Current status

NA62 took its first data in a pilot run in the fall of 2014, and had its first physics run during the summer and fall of 2015. During the 2015 run, the beamline was commissioned up to the full design intensity. The spectrometer, the PID detectors, and all of the photon veto systems were fully operational; the Gigatracker was partially commissioned. By the end of the 2015 run, the infrastructure for the FPGA-programmable level-0 and software level-1 triggers was operational, with trigger conditions and algorithms under study. A data set was collected at low beam intensity (1% of design) with a minimum bias trigger; this data was used to study and verify the performance of the detector, as described below. A data set collected at beam intensities of 50–100% of the design value was also collected and is currently under study.

Selection of a sample of one-track events for efficiency and performance studies proceeds as follows. Events with one positive track in the spectrometer satisfying acceptance and quality cuts and with its origin in the fiducial decay volume are first selected. This track is matched in space and time to hits on the charged hodoscope, RICH rings, and hits in the LKr and muon vetoes, if any. The track is also matched in time to any hits on the photon vetoes or additional hits on the LKr. The spectrometer track is then matched to a track from the Gigatracker, the vertex is formed, and the track from the Gigatracker is matched in time with the signal from the KTAG.

Figure 4, left, shows the distribution of squared missing mass m_{miss}^2 vs. track momentum P_{π^+} for selected one-track events with kaon beam identification from the KTAG. m_{miss}^2 is calculated assuming the track is from a π^+ , and the upper band contains $K^+ \rightarrow \pi^+\pi^0$ events, which peak at $m_{\text{miss}}^2 = m_{\pi^0}^2$. The lower band at $m_{\text{miss}} \approx 0$ at high momentum and curving towards negative values at low track momentum corresponds to the $K^+ \rightarrow \mu^+\nu$ events, for which the track mass hypothesis is incorrect. The concentration of $K^+ \rightarrow \pi^+\pi^+\pi^-$ events is visible at $m_{\text{miss}}^2 > 4m_{\pi^\pm}^2$. The region

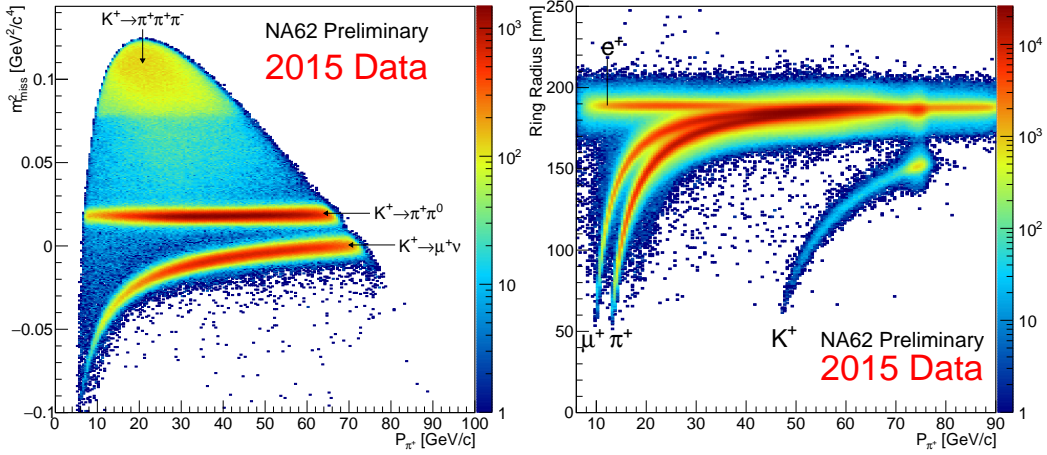


Figure 4: Plots illustrating reconstruction quality for one-track events in NA62 data from the 2015 run. Left: squared missing mass m_{miss}^2 at the presumed $K\pi$ vertex vs. track momentum P_{π^+} measured in the spectrometer. Right: RICH ring radius vs. track momentum P_{π^+} .

between the band from $K^+ \rightarrow \pi^+ \pi^0$ and the concentration from $K^+ \rightarrow \pi^+ \pi^+ \pi^-$ is populated by $K^+ \rightarrow \pi^0 e^+ \nu$ and $K^+ \rightarrow \pi^0 \mu^+ \nu$ decays. Because the signal from the KTAG is required, few events are observed outside the expected regions of correlation from abundant decays. With the beam track reconstructed in the Gigatracker, for a clean LKr-based selection of $K^+ \rightarrow \pi^+ \pi^0$ events, the missing-mass resolution is found to be $\sigma(m_{\text{miss}}^2) = 0.0013 \text{ GeV}^2$, which is near to the design value, and essentially independent of track momentum.

Figure 4, right, shows the distribution of ring radius in the RICH vs. track momentum for selected tracks. The bands of correlation for e , μ , π , and K are clearly visible. Pure samples of pions and muons can be selected using kinematic cuts (see above) and allow the π/μ separation power provided by the RICH and muon veto systems to be measured. Preliminary results indicate that the RICH suppresses muons by a factor of $\sim 10^{-2}$ at 80% efficiency for pions. From a separate analysis, the suppression factor for muons provided by the muon vetoes is $\sim 10^{-6}$ at 50% efficiency or better for pions; the pion efficiency is expected to be further improved. The tracking and particle identification systems can be used together to obtain a clean sample of $K^+ \rightarrow \pi^+ \pi^0$ decays to study the photon veto efficiency. The most directly relevant figure of merit is the overall efficiency for detection of at least one of the two photons from the π^0 in any of the photon vetoes. Thus defined, the π^0 rejection is $\sim 10^{-6}$, but this measurement is limited by the low statistics of the 2015 minimum-bias data set.

4. Broader physics program

In addition to the measurement of $\text{BR}(K^+ \rightarrow \pi^+ \nu \bar{\nu})$, the intense NA62 kaon beam and high-performance NA62 detector will allow the pursuit of a broad program in kaon physics, including precision measurements of dominant K^+ BRs, studies of decays of interest in chiral perturbation theory, and a precision test of lepton universality via the measurement of the ratio $R_K = \Gamma(K_{e2}/K_{\mu 2})$. The sample of 10^{13} K^+ decays will allow searches for lepton-flavor (e.g. $K^+ \rightarrow \pi^+ \mu^\pm e^\mp$) or lepton-number (e.g. $K^+ \rightarrow \pi^- \ell^+ \ell^+$) violating decays with single-event sensitivities

at the level of 10^{-12} . Searches for heavy neutral leptons ν_h can be performed either inclusively, via the missing-mass distribution for $K^+ \rightarrow \ell^+ \nu_h$ decays or via the direct search for ν_h from upstream decays to $\pi^\pm \ell^\mp$. Long-lived dark sector particles produced in the target, such as dark photons (decaying to $\ell^+ \ell^-$) or axion-like particles (decaying to $\gamma\gamma$) can also be searched for. Finally, since $\text{BR}(K^+ \rightarrow \pi^+ \pi^0) \approx 21\%$ and the daughter π^0 is tagged by the reconstruction of the K^+ and π^+ , sensitive searches for rare or forbidden π^0 decays, such as $\pi^0 \rightarrow \text{invisible}$, may also be carried out.

5. Outlook

The 2015 data show that, at low intensity, the detector is fully operational and the key detector systems are largely performing as expected. At the time of writing, the 2016 run is underway (April–November). Additional runs are planned for 2017 and 2018. Work continues on optimizing the trigger algorithms, readout performance, and reconstruction code for running at higher intensities. Assuming the SM value for $\text{BR}(K^+ \rightarrow \pi^+ \nu \bar{\nu})$, the experiment expects to collect a few signal events by the end of 2016 run and is on track to collect ~ 100 events and measure the BR to $\sim 10\%$ by 2018.

References

- [1] V. Cirigliano, G. Ecker, H. Neufeld, A. Pich and J. Portoles, *Rev. Mod. Phys.* **84**, 399 (2012) [arXiv:1107.6001 [hep-ph]].
- [2] A. J. Buras, D. Buttazzo, J. Girrbach-Noe and R. Knegjens, *JHEP* **1511**, 033 (2015) [arXiv:1503.02693 [hep-ph]].
- [3] A. J. Buras, D. Buttazzo and R. Knegjens, *JHEP* **1511**, 166 (2015) [arXiv:1507.08672 [hep-ph]].
- [4] J. K. Ahn *et al.*, arXiv:1609.03637 [hep-ex].
- [5] A. V. Artamonov *et al.* [BNL-E949 Collaboration], *Phys. Rev. D* **79**, 092004 (2009) [arXiv:0903.0030 [hep-ex]].
- [6] F. Hahn *et al.* (eds.) [NA62 Collaboration], “NA62: Technical Design Document,” NA62-10-07 (2010).
- [7] M. Perrin-Terrin [NA62 GTK Working Group], *PoS VERTEX 2015*, 016 (2015).
- [8] H. Danielsson [NA62 Collaboration], 2013 IEEE Nuclear Science Symposium and Medical Imaging Conference, doi:10.1109/NSSMIC.2013.6829462.
- [9] V. Duk, *Int. J. Mod. Phys. Conf. Ser.* **44**, 1660230 (2016).
- [10] E. Goudzovski *et al.*, *Nucl. Instrum. Meth. A* **801**, 86 (2015) [arXiv:1509.03773 [physics.ins-det]].
- [11] F. Ambrosino *et al.*, *IEEE Nucl. Sci. Symp. Conf. Rec.* **2011**, 1159 (2011) [arXiv:1111.4075 [physics.ins-det]].
- [12] V. Fanti *et al.* [NA48 Collaboration], *Nucl. Instrum. Meth. A* **574**, 433 (2007).